A New Synchronous Reference Frame-Based Method for Single-Phase Shunt Active Power Filters

Monfared, Mohammad; Golestan, Saeed; Guerrero, Josep M.

Published in:
Journal of Power Electronics

DOI (link to publication from Publisher):
10.6113/JPE.2013.13.4.692

Publication date:
2013

Document Version
Early version, also known as pre-print

JPE 12-4-10

http://dx.doi.org/10.6113/JPE.2012.12.4.000

A New Synchronous Reference Frame Based Method for Single-Phase Shunt Active Power Filters

Mohammad Monfared*, Saeed Golestan‡ and Josep M. Guerrero†

*Dept. of Electrical Eng., Faculty of Engineering, Ferdowsi University of Mashhad, Mashhad, Iran
‡Dept. of Electrical Eng., Abadan Branch, Islamic Azad University, Abadan, Iran
†Dept. of Energy Technology, Aalborg University, Aalborg, Denmark

Abstract

This paper deals with the design of a novel method in the synchronous reference frame (SRF) to extract the reference compensating current for single-phase shunt active power filters (APFs). Unlike previous works in the SRF, the proposed method has an innovative feature that it does not need the fictitious current signal. Frequency-independent operation, accurate reference current extraction and relatively fast transient response are other key features of the presented strategy. The effectiveness of the proposed method is investigated by means of detailed mathematical analysis. The results confirm the excellent performance of the suggested approach. Theoretical evaluations are confirmed by experimental results.

Key words: Active filter, Synchronous reference frame, Power quality

I. INTRODUCTION

Recently, with ever increasing use of non-linear loads, particularly power electronic equipments, and rising concerns about power quality issues, both energy consumers and electrical supply industry demand for innovative as well as cost-effective power quality enhancement solutions. Traditionally, shunt connected LC passive filters, tuned at dominant harmonic frequencies, have been used to absorb harmonic currents generated by nonlinear loads. Besides their bulky sizes and heavy weights, they suffer from serious technical drawbacks such as: 1) susceptibility to resonances with the load and line impedances; 2) sensitivity to components tolerances and system parameters variations; and 3) possibility of overloading by ambient harmonic loads. Active power filters (APFs) have proved success to overcome the above mentioned problems. An APF is a power electronic converter-based device, designed to compensate for current and voltage disturbances caused by nonlinear loads. Compared to passive filters, APFs offer superior filtering performance, smaller size, and flexibility in application. Although the cost of APFs can be high, the severe harmonic distortion limits has drastically increased the installation and operating costs of passive filters, thus making the option of using APFs economically viable. Many manufacturers have already put APFs on the market and as a results of a strong competition in cost and performance among them, APFs are becoming affordable and can compete well with traditional passive filters in high demand applications [1]. The APFs can be classified as three-phase and single-phase APFs, and this paper focuses on the latter one. The single-phase APF can be used in low and medium power applications, especially in single-phase adjustable speed motor drives, arc furnaces [2], air-conditioning systems [3], electric tractions [4], electronic fluorescent lamp ballasts [5], and so on. In terms of their function, APFs can also be classified into four major categories, namely: (1) shunt APFs; (2) series APFs; (3) hybrid APFs; and (4) the unified power quality conditioner (UPQC) [6].

Generally, a single-phase shunt APF, which is the scope of the present paper, can operate in either perfect harmonic cancellation (PHC) mode or unity power factor (UPF) mode [7]. In PHC mode, the shunt APF is intended to compensate the total harmonic contents demanded by the nonlinear load, while, in UPF mode, besides the harmonic currents, the reactive current component drawn by the nonlinear load should also be compensated.

Fig. 1 shows the schematic diagram of a single-phase shunt APF. As it can be seen, the control system consists of three

Manuscript received Sep. 7, 2012; revised Dec. 4, 2012
Recommended for publication by Associate Editor Hyung-Min Ryu.

*Corresponding Author: m.monfared@um.ac.ir
Tel: +98-511-8805017, Ferdowsi University of Mashhad
‡Dept. of Electronic Eng., Abadan Branch, Islamic Azad University, Abadan, Iran
†Dept. of Energy Technology, Aalborg University, Aalborg, Denmark
joz@et.aau.dk

main parts: 1) reference current generation (RCG) block, which is responsible for extraction of the total harmonic contents and, if required, reactive component of the distorted current drawn by the non-linear load; 2) DC-link voltage control block, which regulates the active power balance between the APF and the grid; and 3) current control block, which generates the appropriate gating signals for the voltage source inverter (VSI), so that the output current of the VSI tracks the reference command delivered by the RCG block.

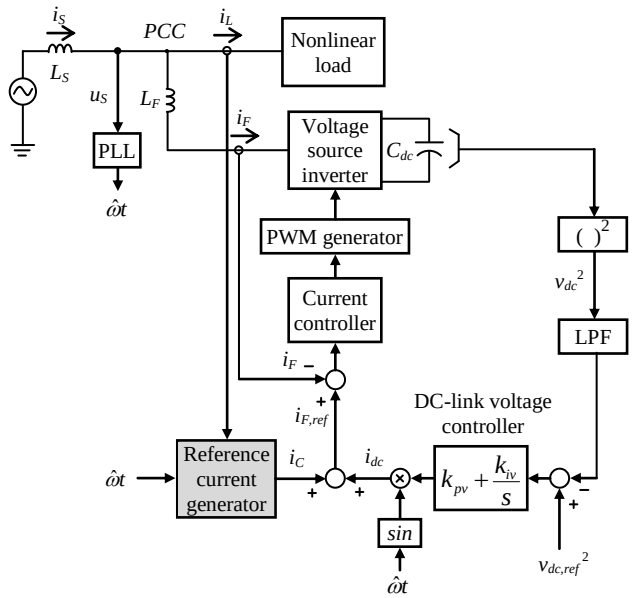

Fig. 1. Schematic diagram of a single-phase shunt APF.

To generate the reference compensating current for single-phase shunt APFs, different techniques can be applied [5]-[13]. Among them, the synchronous reference frame (SRF) or dq theory, which is widely applied to three phase systems, is believed to be one of the simplest and most attractive techniques. The SRF theory offers the potential for achieving fast and accurate extraction of the harmonic contents and reactive component of a distorted current, but the application was dedicated to three-phase APFs. Saitou et al. extended the SRF theory to single-phase APFs [14]. In their method, as shown in Fig. 2, the fundamental component of the single phase signal is shifted by 90^o to generate a fictitious phase signal. Thus, it is possible to represent the single-phase APF as a pseudo two phase (αβ) system. Detailed information on constructing the fictitious phase can be found in [15] and [16]. Although, this technique achieves a desired harmonic compensation, but its implementation suffers from some drawbacks, as follows: Using the Hilbert transform for constructing the fictitious phase, requires a high computational load. On the other hand, due to the sensitivity of the algorithm to the grid frequency fluctuations, any variation in the grid frequency introduces an error in the calculated reference current. In addition, the reactive power compensation is not considered in this method.

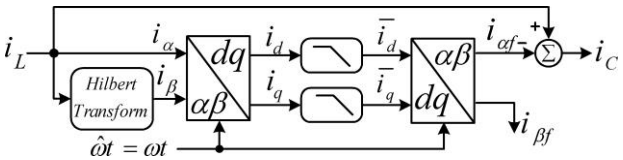

Fig. 2. Basic scheme of the SRF harmonic extraction technique [14].

To overcome some of the aforementioned drawbacks, Kim et al. have proposed a control technique; we call it double synchronous reference frame (DSRF) method [17]. In DSRF, the fictitious phase is constructed by using a low-pass filter, and two SRF, dq^+ and dq^-, rotating in the opposite directions, are utilized for generating the reference current. In the following section, it will be shown that, from the control point of view, the DSRF method is equivalent to the control technique depicted in Fig. 2, except that the fictitious phase (β-axis signal) has been set to zero. The poor performance in reactive power compensation, and imposing an unnecessary complexity and high computational burden to the control system will then be concluded as the main drawbacks of DSRF method.

As discussed above, the fictitious current signal is a common feature in all previously reported RCG techniques in the SRF. The objective of this paper is to present a novel RCG technique in SRF, which does not need the fictitious current signal. Frequency-independent operation, accurate reference current extraction and relatively fast transient response are other key features of the suggested algorithm. A detailed analysis of the proposed strategy in different operating conditions of a shunt APF is presented. The results indicate the excellent performance of the proposed method. The theoretical evaluations are confirmed through experiments.

II. Review of DSRF Method and Introduction to Proposed Method

Fig. 3 shows the basic scheme of the DSRF method [17]. In Fig. 3, $i_{\alpha f}$ and i_C are the extracted fundamental and harmonic components of the nonlinear load current, respectively.

Moving the sums ahead of the LPFs, yields Fig. 4. From Fig. 4, the following equations can be obtained:

$$i_d = i_{d,pos} - i_{d,neg} \tag{1}$$

$$i_q = i_{q,pos} + i_{q,neg} \tag{2}$$

Transforming from the αβ reference frame into the dq^+ and dq^- reference frame is described by the following two matrix equations, respectively [17].

$$\begin{bmatrix} i_{d,pos} \\ i_{q,pos} \end{bmatrix} = T(t) \begin{bmatrix} i_\alpha \\ i_\beta \end{bmatrix} \tag{3}$$

$$\begin{bmatrix} i_{d,neg} \\ i_{q,neg} \end{bmatrix} = T(-t) \begin{bmatrix} i_\alpha \\ i_\beta \end{bmatrix} \tag{4}$$

where,

$$T(t)=\begin{bmatrix}\sin(\omega t) & -\cos(\omega t)\\ -\cos(\omega t) & -\sin(\omega t)\end{bmatrix} \quad (5)$$

By substituting (3) and (4) into (1) and (2), i_d and i_q can be written as follows:

$$i_d = 2\sin(\omega t)i_\alpha \quad (6)$$

$$i_q = -2\cos(\omega t)i_\alpha \quad (7)$$

In matrix form, (6) and (7) can be rewritten as:

$$\begin{bmatrix}i_d\\ i_q\end{bmatrix}=\begin{bmatrix}\sin(\omega t) & -\cos(\omega t)\\ -\cos(\omega t) & -\sin(\omega t)\end{bmatrix}\begin{bmatrix}2i_\alpha\\ 0\end{bmatrix}=T(t)\begin{bmatrix}2i_\alpha\\ 0\end{bmatrix} \quad (8)$$

Using above matrix equation, the DSRF method shown in Fig. 4, can be further simplified, as shown in Fig. 5.

Notice that, from the control point of view, the control structure shown in Fig. 5 is exactly equivalent to the DSRF technique shown in Fig. 3. Thus, it can be concluded that the DSRF method imposes an unnecessary complexity and high computational burden on the control system.

The drawbacks of the DSRF method are further investigated by using a simple mathematical analysis, as follows.

Let the nonlinear load current be represented by [11]:

$$i_L = I_m \sin(\omega t-\phi)+\sum_{k=3,5,7,..} I_k \sin(k\omega t-\phi_k) \quad (9)$$

where, ω is the grid voltage fundamental frequency, I_m and ϕ are the amplitude and phase of the fundamental current, respectively, and I_k and ϕ_k are the magnitude and the phase of the k^{th} harmonic-current component, respectively.

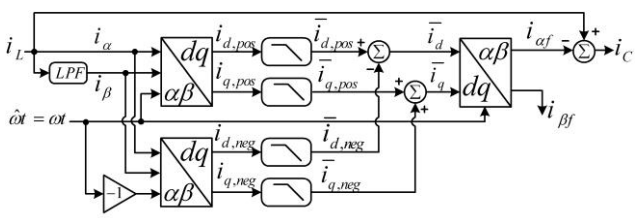

Fig. 3. Basic scheme of DSRF method [17].

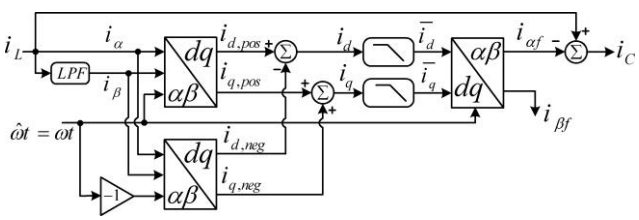

Fig. 4. Simplification of DSRF method using block diagram algebra.

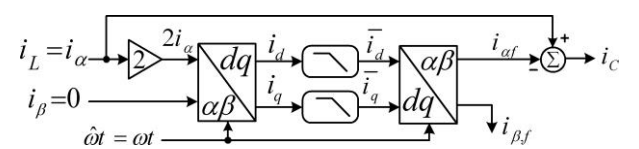

Fig. 5. Simplified equivalent of DSRF method.

By substituting (9) into (6) and (7), i_d and i_q can be obtained as:

$$i_d = I_m\cos(\phi)-I_m\cos(2\omega t-\phi) + \sum_{k=3,5,7,..} I_k\left[\cos((k-1)\omega t-\phi_k)-\cos((k+1)\omega t-\phi_k)\right] \quad (10)$$

$$i_q = I_m\sin(\phi)-I_m\sin(2\omega t-\phi) - \sum_{k=3,5,7,..} I_k\left[\sin((k-1)\omega t-\phi_k)-\sin((k+1)\omega t-\phi_k)\right] \quad (11)$$

where, the constant terms $I_m cos(\phi)$ and $I_m sin(\phi)$ are corresponding to the magnitude of the active and reactive currents of the nonlinear load, respectively.

From (10) and (11), it can be seen that i_d and i_q contain significant 2^{nd}-order harmonic contents, thus, their removal requires the use of either a first (or second) order LPF with a low cutoff frequency, or a high-order LPF. Using a high-order LPF, besides the stability problems, imposes a high computational load on the control system [18]. On the other hand, using a low-order LPF with a low cutoff frequency significantly degrades the transient performance of the APF.

In the light of the foregoing analysis, the efficiency of the control technique claimed by Kim et al. [17] is significantly undermined.

To cancel out these undesired double-frequency oscillations without degrading the stability and transient performance of the system, a novel method, called double-frequency oscillation cancellation (DFOC) method, is presented in this paper. The performance of this method is then investigated by means of detailed mathematical analysis.

III. DFOC METHOD

In this section, the main focus is on eliminating the double-frequency ripples $I_m cos(2\omega t-\phi)$ and $I_m sin(2\omega t-\phi)$ from i_d and i_q, respectively. Thus, for the sake of simplicity, i_d and i_q are considered as:

$$i_d = I_m\cos(\phi)-I_m\cos(2\omega t-\phi) \quad (12)$$

$$i_q = I_m\sin(\phi)-I_m\sin(2\omega t-\phi) \quad (13)$$

Expanding (12) and (13) gives

$$i_d = I_m\cos(\phi)-I_m\cos(\phi)\cos(2\omega t)-I_m\sin(\phi)\sin(2\omega t) \quad (14)$$

$$i_q = I_m\sin(\phi)+I_m\sin(\phi)\cos(2\omega t)-I_m\cos(\phi)\sin(2\omega t) \quad (15)$$

Notice that, the amplitudes of the double-frequency oscillation terms depend on the average value of i_d and i_q. The perfect cancellation of these undesired components can be easily achieved by injecting double-frequency signals with the same amplitude but opposite phase angle into i_d and i_q. Fig. 6 illustrates the schematic diagram of the proposed strategy, where, $\hat{\omega}$ denotes the estimated frequency by the PLL, and

throughout this section we will assume that $\hat{\omega}=\omega$. The LPF block is considered as a first-order LPF, as follows:

$$LPF(s)=\frac{\omega_c}{s+\omega_c} \tag{16}$$

where, ω_c is the cut-off frequency of the LPF.

To analyze the performance of the proposed method, the mathematical expressions for $\bar{i}_d$ and $\bar{i}_q$ are derived:

$$\begin{aligned}\bar{i}_d = A_d + \{&B_d\cos(\omega t)\cos(\omega_f t)\\ &+C_d\sin(\omega t)\sin(\omega_f t)\\ &+D_d\sin(\omega t)\cos(\omega_f t)\\ &+E_d\cos(\omega t)\sin(\omega_f t)\}e^{-\omega_c t}\end{aligned} \tag{17}$$

$$\begin{aligned}\bar{i}_q = A_q + \{&B_q\cos(\omega t)\cos(\omega_f t)\\ &+C_q\sin(\omega t)\sin(\omega_f t)\\ &+D_q\sin(\omega t)\cos(\omega_f t)\\ &+E_q\cos(\omega t)\sin(\omega_f t)\}e^{-\omega_c t}\end{aligned} \tag{18}$$

where,

$\omega_f=\sqrt{\omega^2-\omega_c^2}$,

$A_d=-B_d=-D_q=I_m\cos(\phi)$,

$C_d=-E_q=-I_m\left[\omega\cos(\phi)+\omega_c\sin(\phi)\right]/\omega_f$,

$D_d=A_q=-B_q=I_m\sin(\phi)$, and

$E_d=C_q=-I_m\left[\omega_c\cos(\phi)+\omega\sin(\phi)\right]/\omega_f$.

Detailed derivation of (17) and (18) can be found in the Appendix A.

In order to highlight the advantages of the proposed method, the mathematical expressions for $\bar{i}_d$ and $\bar{i}_q$ without using the DFOC block are also presented. These expressions are as follows:

$$\begin{aligned}\bar{i}_d = I_m\cos(\phi)-(&A'_d+I_m\cos\phi)e^{-\omega_c t}\\ &+A'_d\cos(2\omega t)+B'_d\sin(2\omega t)\end{aligned} \tag{19}$$

$$\begin{aligned}\bar{i}_q = I_m\sin(\phi)-(&A'_q+I_m\sin\phi)e^{-\omega_c t}\\ &+A'_q\cos(2\omega t)+B'_q\sin(2\omega t)\end{aligned} \tag{20}$$

where,

$A'_d=B'_q=I_m\omega_c(2\omega\sin\varphi-\omega_c\cos\phi)/(4\omega^2+\omega_c^2)$, and

$B'_d=-A'_q=-I_m\omega_c(2\omega\cos\phi+\omega_c\sin\varphi)/(4\omega^2+\omega_c^2)$.

From (17) and (18) it can be seen that, the fluctuating terms decay to zero with a time constant of $1/\omega_c$, and $\bar{i}_d$ and $\bar{i}_q$ converge to $I_m\cos(\phi)$ and $I_m\sin(\phi)$, respectively. However, in (19) and (20), $\bar{i}_d$ and $\bar{i}_q$ contain high amplitude double-frequency contents. These results are clearly illustrated in Fig. 7 for $I_m=10$ A, $\phi=\pi/3$ rad, $\omega_c=50$ rad/s, and $\omega=100\pi$ rad/s. As expected, using the DFOC block, the perfect cancellation of double-frequency harmonics is achieved.

IV. Application of the DFOC Method in Different Control Modes of a Shunt APF

The aim of this section is to investigate the application of the DFOC block for extraction of the reference compensating current in different control strategies of a shunt APF (i.e. UPF and PHC modes of operation).

A. PHC Mode

Fig. 8 shows the application of the DFOC block to extract the reference compensating current in the PHC mode of operation. Notice that the suggested strategy eliminates the need for the fictitious current signal.

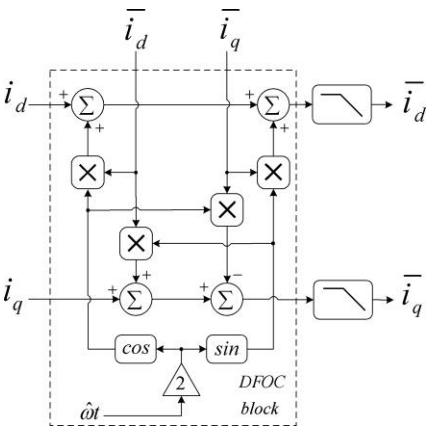

Fig. 6. Schematic diagram of DFOC method.

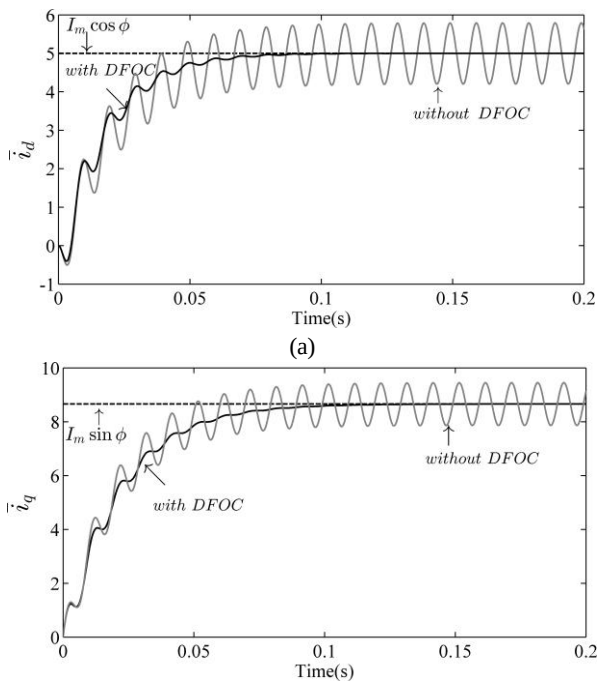

Fig. 7. Comparative results for $\bar{i}_d$ and $\bar{i}_q$. (a) $\bar{i}_d$ with (black line) and without (gray line) using DFOC block. (b) $\bar{i}_q$ with (black line) and without (gray line) using DFOC block.

To analyze the performance of the proposed method, the transfer function of the extracted fundamental current to the load current is presented, as follows:

$$G_{DFOC} = \frac{i_{\alpha f}}{i_L} = \frac{2\omega_c s}{s^2 + 2\omega_c s + \omega^2} \quad (21)$$

Detailed derivation of (21) can be found in Appendix B.

Fig. 9 shows the bode plot of the transfer function (21) for three different values of cutoff frequency ω_c. We observe that the transfer function (21) exhibits a band-pass filtering behavior with a pass-band centered at the fundamental frequency. Notice that, the bandwidth of the band-pass filter (BPF) is proportional to the cut-off frequency of the LPF. The lower the cut-off frequency, the less is the BPF bandwidth, and the better is the filtering performance.

The transient behavior of the proposed algorithm can be analyzed by determining the closed loop poles of the transfer function (21), as follows:

$$p_1 = -\omega_c + j\,\omega,\ p_2 = -\omega_c - j\,\omega \quad (22)$$

As it can be seen in (22), the transient time of the algorithm is dictated by the cut-off frequency of the LPF. The higher the cutoff frequency, the faster is the transient response [19]-[21].

The dc-offset rejection capability is another important feature that must be examined. As it can be seen in (21), the transfer function G_{DFOC} has a zero located at the origin, thus, for all values of ω_c, the perfect rejection of the dc-offset is achieved.

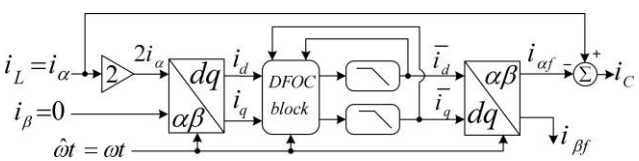

Fig. 8. Proposed method to extract the reference compensating current in PHC mode of a shunt APF.

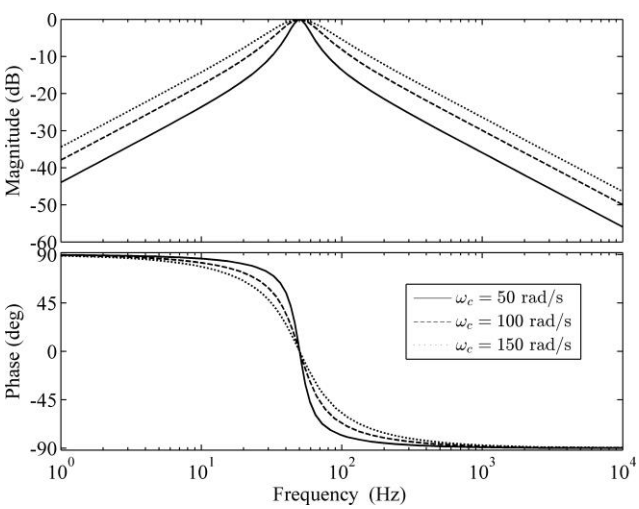

Fig. 9. Bode diagram of transfer function (21) for three different values of cutoff frequency ω_c.

Finally, the performance of the proposed algorithm is investigated under grid frequency deviations. Notice that the transfer function of (21) is derived by assumption that $\hat{\omega} = \omega$. Without this assumption, it can be easily demonstrated that the transfer function of the extracted fundamental current to the load current is:

$$G_{DFOC} = \frac{2\omega_c s}{s^2 + 2\omega_c s + \hat{\omega}^2} \quad (23)$$

Substituting the Laplace operator $s = j\,\omega$ into (23) yields:

$$G_{DFOC}\big|_{s=j\,\omega} = \frac{j\,2\omega_c \omega}{\hat{\omega}^2 - \omega^2 + j\,2\omega_c \omega} \quad (24)$$

From (24) it is evident that, under grid frequency variations, if the estimated frequency by the PLL is very close (or preferably equal) to the actual one, the perfect extraction of the fundamental-current component, and hence, the accurate reference compensating current is achieved.

B. UPF Mode

Fig. 10 shows the application of the DFOC block to extract the reference compensating current in the UPF mode of operation of a single-phase shunt APF, where, i_p denotes the extracted active current drawn by the load. In a procedure similar to that discussed in section IV-A, we can realize the same operational characteristics for the system of Fig. 10, as follows: 1) frequency-independent operation; and 2) dependency of the transient response and the filtering accuracy to the value of cutoff frequency of the LPF.

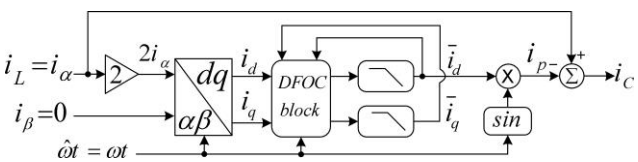

Fig. 10. Proposed method to extract the reference compensating current in UPF mode of a shunt APF.

V. Output Current and DC-link Voltage Controllers

It is clear from the control scheme of Fig. 1 that the performance of the APF system highly depends on the quality of the current controller. If the converter model in Fig. 1 is simplified to $1/(L_F s + R_F)$, where L_F and R_F are the filter inductance and resistance, respectively, and assuming that the current controller is composed of $k_{pc} + k_{ic}/s$ (Fig. 11(a)), then the closed-loop transfer function of the current controller can be easily derived as:

$$\frac{i_F}{i_{F,ref}} = \frac{k_{pc} s + k_{ic}}{Ls^2 + (R + k_{pc})s + k_{ic}} \quad (25)$$

where i_F and $i_{F,ref}$ are the measured and reference currents for the APF, respectively. Obviously, the choice of controller

gains is a compromise between the stability margin and the dynamic performance. In this work the bandwidth is chosen to be 2 kHz which is enough to effectively cover up to 39rd harmonics, and also is much lower than the switching frequency to prevent the sensitivity to the switching noises.

On the other hand, as depicted in Fig. 1, a controller must regulate the DC-link voltage in order to keep the energy balance between the APF and the grid. Practically, converter losses and the leakage of the DC-link capacitors cause the active filter to draw a fundamental active component to maintain the DC-link voltage at its predefined value [22]-[25]. The DC-link voltage controller is adopted from [3], in which the small-signal model of the DC-link voltage loop is derived as presented in Fig. 11(b), where C_{dc} is the total DC-link capacitance, U_{ps} is the peak value of the PCC voltage, ω_{cv} = 60 rad/s is the cutoff frequency of the low-pass filter, and k_{pv} and k_{iv} are the gains of the PI regulator.

To avoid interaction between the DC-link voltage and the output current controllers, the bandwidth of the voltage loop is chosen much below that of the current loop. Indeed, a bandwidth not bigger than one tenth of grid frequency and a phase margin in the range of 30° to 60° is recommended [3].

VI. Experimental Results

To confirm the performance of the proposed algorithm, the system shown in Fig. 1 has been developed in the laboratory. A TMS320F28335 digital signal controller (DSC) from the Texas Instruments is used to perform the algorithm and generate the proper gating signals for the single phase converter. Table I shows the salient parameters of the system. For all experiments, the cutoff frequency of the LPF is chosen to be 95 rad/s.

As a worst case operation, the performance of the proposed APF system has been investigated in presence of a highly nonlinear load consisting of a diode rectifier bridge feeding a capacitor in parallel with a resistor. As shown in Fig. 12, the load current is highly distorted with zero periods, while the source current remains sinusoidal and in-phase with the grid voltage. The current quality can be further improved by using the DFOC block. In this case, the THD is reduced to 4.18% and the lowest order harmonic (3rd harmonic) is attenuated drastically.

In another study, depicted in Fig. 13, a resistive load is in service, and the system is at steady state. Suddenly, a nonlinear rectifier load is switched on. Obviously, the transient period is around two cycles of the fundamental frequency, which is fairly longer than that the time required for the FFT method [26], almost equal to that of [27], and shorter compared to that of [28]. The source current and the grid voltage are initially in-phase and after the transient period, the phase difference is again converged to zero in the steady state, which means the unity power factor is achieved.

Table II summarize the transient time and THD of the source current with the same resistive plus rectifier load used for Fig. 13, and for different values of the cutoff frequency of the LPF. As expected, the higher the cutoff frequency, the faster is the transient response, and at the same time the higher is the THD.

In the last study, shown in Fig. 14, the load on the system is suddenly changed about 200% and as it can be seen the DC-link voltage recovers in about 400 ms with a smooth transient performance, confirming the slow bandwidth with enough stability margin of the DC-link voltage loop.

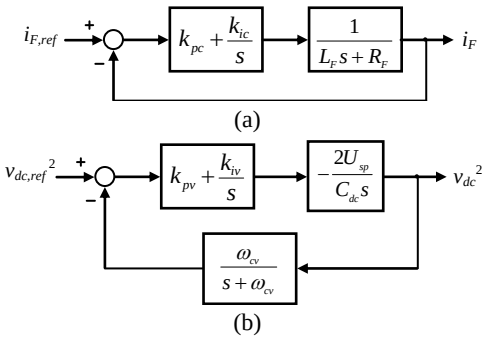

Fig. 11. Small signal model of (a) output current, and (b) DC-link voltage loops [3].

TABLE I
System Parameters

Quantity	Description	Value
u_s	AC power source voltage (rms)	110 V
f	AC power source frequency	50 Hz
L_s	Grid inductance	80 μH
C_{dc}	DC capacitance	4800 μF
f_s	Switching frequency	20 kHz
f_{sam}	Sampling frequency	40 kHz
L_F	Filter inductance	2.5 mH
R_F	Filter resistance	0.5 Ω

TABLE II
THD and Transient Time of the Source Current for Different Values of the Cutoff Frequency of LPF

ω_c (rad / s)	THD (%)	Transient time (ms)
50	1.91	45
75	2.44	30
100	2.50	24
125	2.52	15
150	2.75	12

VII. Conclusions

A novel method in the synchronous reference frame for extraction of the reference compensating current for single phase APFs has been proposed. The major advantages of the proposed technique can be summarized as:

- Simple algorithm;
- No need for the fictitious current signal;
- Frequency-independent operation;
- Accurate reference current extraction;
- Fast transient response.

The effectiveness of the proposed method is investigated by detailed mathematical analysis and is confirmed through experiments.

APPENDIX

A. Derivation of the Mathematical Expressions for $\bar{i}_{dq}$ [Fig. 6]

From Fig. 6, in the Laplace domain, we obtain:

$$\bar{i}_d(s) = \frac{\omega_c}{s+\omega_c} \times \ell\left[i_d(t) + \bar{i}_d(t)\cos(2\omega t) + \bar{i}_q(t)\sin(2\omega t)\right] \quad (26)$$

$$\bar{i}_q(s) = \frac{\omega_c}{s+\omega_c} \times \ell\left[i_q(t) + \bar{i}_d(t)\sin(2\omega t) - \bar{i}_q(t)\cos(2\omega t)\right] \quad (27)$$

where, ℓ denotes the Laplace operator.

Multiplying both sides of (26) and (27) by $(s+\omega_c)$, and rearranging, gives:

$$\bar{i}_d(s) = \omega_c \times \ell\left[i_d(t) + (\cos(2\omega t)-1)\bar{i}_d(t) + \sin(2\omega t)\bar{i}_q(t)\right] \quad (28)$$

$$\bar{i}_q(s) = \omega_c \times \ell\left[i_q(t) + \sin(2\omega t)\bar{i}_d(t) - (\cos(2\omega t)+1)\bar{i}_q(t)\right] \quad (29)$$

Converting (28) and (29) into the time-domain, and rearranging the results into matrix form, yields:

$$\begin{bmatrix} \dot{\bar{i}}_d(t) \\ \dot{\bar{i}}_q(t) \end{bmatrix} = \omega_c \begin{bmatrix} \cos(2\omega t)-1 & \sin(2\omega t) \\ \sin(2\omega t) & -\cos(2\omega t)-1 \end{bmatrix} \begin{bmatrix} \bar{i}_d(t) \\ \bar{i}_q(t) \end{bmatrix} + \begin{bmatrix} \omega_c & 0 \\ 0 & \omega_c \end{bmatrix} \begin{bmatrix} i_d(t) \\ i_q(t) \end{bmatrix} \quad (30)$$

Substituting (12) and (13) into (30), and making some rearrangement, gives:

$$\begin{bmatrix} \dot{\bar{i}}_d(t) \\ \dot{\bar{i}}_q(t) \end{bmatrix} = \omega_c \begin{bmatrix} \cos(2\omega t)-1 & \sin(2\omega t) \\ \sin(2\omega t) & -\cos(2\omega t)-1 \end{bmatrix} \left\{ \begin{bmatrix} \bar{i}_d(t) \\ \bar{i}_q(t) \end{bmatrix} - \begin{bmatrix} I_m\cos(\phi) \\ I_m\sin(\phi) \end{bmatrix} \right\} \quad (31)$$

From (31), the state-space description of the DFOC method can be derived, as follows:

$$\begin{cases} \dot{x}(t) = A(t).x(t) + B(t).u(t) \\ y(t) = C.x(t) \end{cases} \quad (32)$$

where

$$x(t) = \begin{bmatrix} \bar{i}_d(t) \\ \bar{i}_q(t) \end{bmatrix}; \quad u(t) = \begin{bmatrix} I_m\cos(\phi) \\ I_m\sin(\phi) \end{bmatrix}$$

$$A(t) = -B(t) = \omega_c \begin{bmatrix} \cos(2\omega t)-1 & \sin(2\omega t) \\ \sin(2\omega t) & -\cos(2\omega t)-1 \end{bmatrix}$$

$$C(t) = I$$

The state-space equation (32), describes a two-input, two-output, linear time-variant system. The analytical solution of (32) is very complicated, and is out of the scope of this paper. Thus, in this paper, the final solution of the state-space equation (32), i.e. (17) and (18), is only presented. Detailed information on solving the linear time-variant systems can be found in [20] and [21].

B. Determination of the Transfer Function between $i_{\alpha f}$ and i_L [Fig. 8]

Substituting (6) and (7) into (30), yields:

$$\begin{bmatrix} \dot{\bar{i}}_d(t) \\ \dot{\bar{i}}_q(t) \end{bmatrix} = A(t).\begin{bmatrix} \bar{i}_d(t) \\ \bar{i}_q(t) \end{bmatrix} + 2\omega_c \begin{bmatrix} \sin(\omega t) \\ -\cos(\omega t) \end{bmatrix} \quad (33)$$

From Fig. 8, we have:

$$\begin{bmatrix} \bar{i}_d(t) \\ \bar{i}_q(t) \end{bmatrix} = T(t) \begin{bmatrix} i_{\alpha f}(t) \\ i_{\beta f}(t) \end{bmatrix} \quad (34)$$

Substituting (33) into (32), gives:

$$\frac{d}{dt}\left\{ T(t).\begin{bmatrix} i_{\alpha f}(t) \\ i_{\beta f}(t) \end{bmatrix} \right\} = A(t)T(t).\begin{bmatrix} i_{\alpha f}(t) \\ i_{\beta f}(t) \end{bmatrix} + 2\omega_c \begin{bmatrix} \sin(\omega t) \\ -\cos(\omega t) \end{bmatrix} i_L \quad (35)$$

Expanding the left-hand side term of (35), making some rearrangement, and multiplying both sides by $T(t)^{-1}$, yields:

$$\frac{d}{dt}\begin{bmatrix} i_{\alpha f}(t) \\ i_{\beta f}(t) \end{bmatrix} = T(t)^{-1}.\left(A(t)T(t) - \frac{dT(t)}{dt} \right).\begin{bmatrix} i_{\alpha f}(t) \\ i_{\beta f}(t) \end{bmatrix} + 2\omega_c T(t)^{-1}\begin{bmatrix} \sin(\omega t) \\ -\cos(\omega t) \end{bmatrix}.i_L \quad (36)$$

where, $T(t)^{-1}$ denotes the inverse of the matrix $T(t)$.

After some simple mathematical manipulations, we have:

$$\frac{d}{dt}\begin{bmatrix} i_{\alpha f}(t) \\ i_{\beta f}(t) \end{bmatrix} = \begin{bmatrix} -2\omega_c & -\omega \\ \omega & 0 \end{bmatrix}.\begin{bmatrix} i_{\alpha f}(t) \\ i_{\beta f}(t) \end{bmatrix} + \begin{bmatrix} 2\omega_c \\ 0 \end{bmatrix}.i_L \quad (37)$$

Considering $i_{\alpha f}$ as the output signal, the state-space representation of the proposed method can be expressed as:

$$\begin{cases} \dot{x}(t) = A'(t).x(t) + B'(t)u(t) \\ y(t) = C'.x(t) \end{cases} \quad (38)$$

where

$$x(t) = \begin{bmatrix} i_{\alpha f}(t) \\ i_{\beta f}(t) \end{bmatrix}; \quad u(t) = i_L$$

$$A'(t) = \begin{bmatrix} -2\omega_c & -\omega \\ \omega & 0 \end{bmatrix}; \; B'(t) = \begin{bmatrix} 2\omega_c \\ 0 \end{bmatrix}$$

$$C'(t) = \begin{bmatrix} 1 & 0 \end{bmatrix}$$

The state-space equation (38), describes a single-input, single-output, linear time-invariant system. Thus, the system transfer function can be obtained, as follows:

$$G_{DFOC} = \frac{i_{\alpha f}(s)}{i_L(s)} = C'\left[sI - A'\right]^{-1}B' = \frac{2\omega_c s}{s^2 + 2\omega_c s + \omega^2} \quad (39)$$

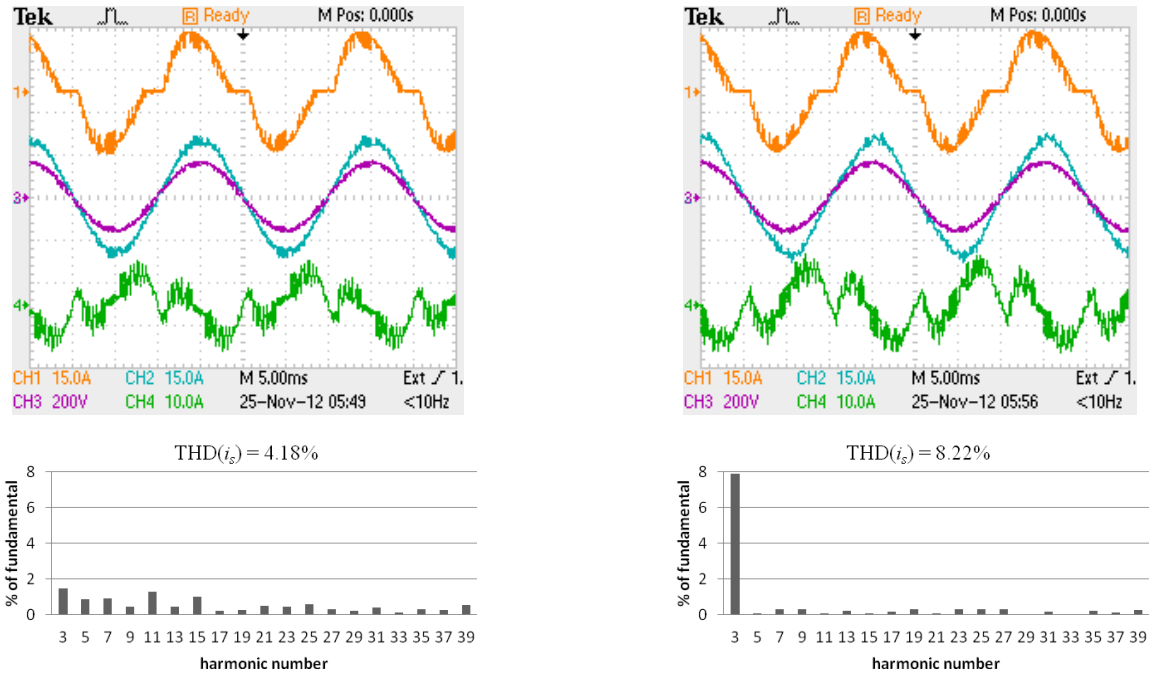

(a) (b)

Fig. 12. Experimental waveforms and harmonic spectrum of source current under a highly nonlinear load (a) with, and (b) without using DFOC block: (CH1) load current, (CH2) source current, (CH3) grid voltage, and (CH4) APF output current.

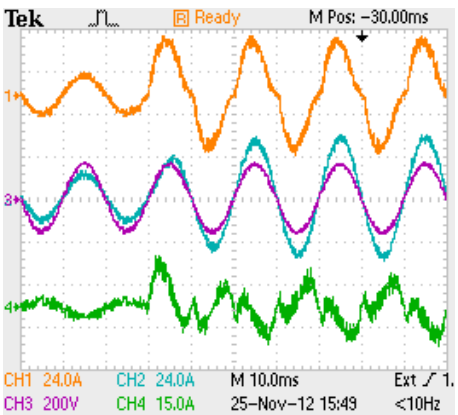

Fig. 13. Experimental waveforms when a rectifier load is added to the resistive load: (CH1) to (CH4) as described in Fig. 12.

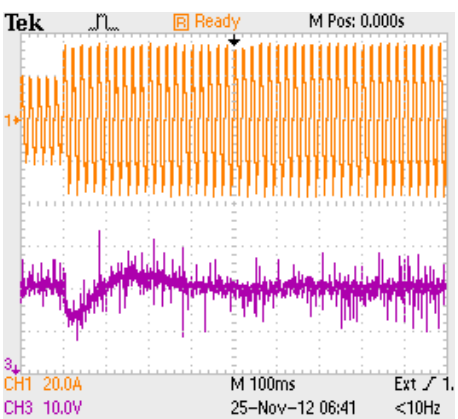

Fig. 14. Experimental waveforms in response to a step load change: (CH1) load current, and (CH3) DC-link voltage.

ACKNOWLEDGMENT

This work was supported in part by Research Deputy of Ferdowsi University of Mashhad, under grant no. 2/22211 (dated 10 July 2012). This support is gratefully acknowledged.

REFERENCES

[1] H. Akagi, "The state-of-the-art of active filters for power conditioning," *in Proc. EPE '05*, pp. P1-P15, 2005.

[2] B. Singh, Al-Haddad K., and A. Chandra, "A review of active power filters for power quality improvement," *IEEE Trans. Ind. Electron.*, Vol. 45, No. 5, pp. 960-971, 1999.

[3] J. Miret, M. Castilla, J. Matas, J. M. Guerrero, and J. C. Vasquez, "Selective harmonic-compensation control for single-phase active power filter with high harmonic rejection," *IEEE Trans. Ind. Electron.*, Vol. 56, No. 8, pp. 3117-3127, Aug. 2009.

[4] L. Ruomei, "A high power active filter for harmonic compensation in an electric locomotive," *in Proc. PowerCon '02*, pp. 1059-1063, 2002.

[5] V. Khadkikar, A. Chandra, and B. N. Singh, "Generalised single-phase p-q theory for active power filtering: Simulation and DSP-based experimental investigation," *IET Power Electron.*, Vol. 2, No. 1, pp. 67-78, Jan. 2009.

[6] M. Cirrincione, M. Pucci, and G. Vitale, "A single-phase DG generation unit with shunt active power filter capability by adaptive neural filtering," *IEEE Trans. Ind. Electron.*, Vol. 55, No. 5, pp. 2093-2110, May 2008.

[7] K. R. Uyyuru, M.K. Mishra, and A. Ghosh, "An optimization-based algorithm for shunt active filter under distorted supply voltages," *IEEE Trans. Power Electron.*,

Vol. 24, No. 5, pp. 1223-1232, May 2009.
[8] M. Rukonuzzaman, and M. Nakaoka, "Single-phase shunt active power filter with harmonic detection," *in Proc. Electr. Power Appl. '02*, pp. 343-350, 2002.
[9] B. M. Han, B. Y. Bae, and S. J. Ovaska, "Reference signal generator for active power filters using improved adaptive predictive filter," *IEEE Trans. Ind. Electron.*, Vol. 52, No. 2, pp. 576-584, Apr. 2005.
[10] P. Kumar, and A. Mahajan, "Soft computing techniques for the control of an active power filter," *IEEE Trans. Power Del.*, Vol. 24, No. 1, pp. 452-461, Jan. 2009.
[11] F. D. Freijedo, J. D. Gandoy, O. Lopez, P. F. Comesana, and C. M. Penalver, "A signal-processing adaptive algorithm for selective current harmonic cancellation in active power filters," *IEEE Trans. Ind. Electron.*, Vol. 56, No. 8, pp. 2829-2840, Aug. 2009.
[12] L. P. Kunjumuhammed, and M. K. Mishra, "Comparison of single phase shunt active power filter algorithms," *in Proc. Annu. Conf. IEEE Power India*, 2006.
[13] S. A. Gonzalez, R. G. Retegui, and M. Benedetti, "Harmonic computation technique suitable for active power filters," *IEEE Trans. Ind. Electron.*, Vol. 54, No. 5, pp. 2791-2796, Oct. 2007.
[14] M. Saitou, N. Matsui, and T. Shimizu, "A control strategy of single phase active filter using a novel d-q transformation," *in Proc. IEEE IAS '03*, pp. 1222-1227, 2003.
[15] J.-W. Choi, Y.-K. Kim, and H.-G. Kim. "Digital PLL control for single-phase photovoltaic system," *in Proc. Electr. Power Appl. '06*, pp. 40-46, 2006.
[16] S. M. Silva, B. M. Lopes, B. J. C. Filho, R. P. Campana, and W. C. Bosventura, "Performance evaluation of PLL algorithms for single phase grid-connected systems," *in Proc. IAS '04*, pp. 2259-2263, 2004.
[17] J. S. Kim, and Y.S. Kim, "A new control method for a single-phase hybrid active power filter based on a rotating reference frame," *Journal of Power Electronics*, Vol. 9, No. 5, pp. 718-725, Sep. 2009.
[18] C. H. Ng, K. Busawon, G. A. Putrus, and L. Ran, "Fast-individual-harmonic-extraction technique," *in Proc. Gener. Transm. Distrib. '05*, pp. 556-562, 2005.
[19] R. C. Dorf, and R. H. Bishop, *Modern Control Systems*, Prentice-Hall, New Jersey, 2001.
[20] T. Kailath, *Linear Systems*, Prentice-Hall, New York, 1980.
[21] C. T. Chen, *Introduction to Linear System Theory*, Holt Rinehart and Winston Inc., New York, 1970.
[22] Y. Han, and L. Xu, "Design and implementation of a robust predictive control scheme for active power filters," *Journal of Power Electronics*, Vol. 11, No. 5, pp. 751-758, Sep. 2011.
[23] J. H. Lee, J. K. Jeong, B. M. Hany, and B. Y. Bae, "New reference generation for a single-phase active power filter to improve steady state performance," *Journal of Power Electronics*, Vol. 10, No. 4, pp. 412-418, Jul. 2010.
[24] H. H. Tumbelaka, L. J. Borle, C. V. Nayar, and S. R. Lee, "A grid current-controlling shunt active power filter," *Journal of Power Electronics*, Vol. 9, No. 3, pp. 365-376, May 2009.
[25] M. Adel, S. Zaid, and O. Mahgoub, "Improved active power filter performance based on an indirect current control technique," *Journal of Power Electronics*, Vol. 11, No. 6, pp. 931-937, Nov. 2011.
[26] L. Asiminoaei, F. Blaabjerg, and S. Hansen, "Detection is key-Harmonic detection methods for active power filter applications," *IEEE Ind. Appl. Mag.*, Vol. 13, No. 4, pp. 22-33, Jul./Aug. 2007.
[27] M. K. Ghartemani, H. Mokhtari, M. R. Iravani, and M. Sedighy, "A signal processing system for extraction of harmonics and reactive current of single phase systems", *IEEE Trans. Power Deliv.*, Vol. 19, pp. 979-986, jul. 2004.
[28] J. S. Tepper, J. W. Dixon, G. Venegas, and L. Morán, "A simple frequency-independent method for calculating the reactive and harmonic current in a nonlinear load," *IEEE Trans. Power Electron.*, Vol. 43, pp. 647-653, Dec. 1996.

Mohammad Monfared received the B.Sc. degree in electrical engineering from Ferdowsi University of Mashhad, Iran, in 2004, and the M.Sc. and Ph.D. degrees (both with honors) in electrical engineering from Amirkabir University of Technology, Tehran, Iran, in 2006 and 2010, respectively.
He is currently an Assistant Professor at Ferdowsi University of Mashhad, Iran. His research interests include power electronics, motor drives, renewable energy systems, energy conversion, and control and applications.

Saeed Golestan received the B.Sc. degree in electrical engineering from Shahid Chamran University of Ahvaz, Iran, in 2006, and the M.Sc. degree in electrical engineering from Amirkabir University of Technology, Tehran, Iran, in 2009.
He is currently a Lecturer with the Department of Electrical Engineering, Abadan Branch, Islamic Azad University, Iran. His research interests include power quality, and distributed generation systems.

Josep M. Guerrero was born in Barcelona, Spain, in 1973. He received the B.S. degree in telecommunications engineering, the M.S. degree in electronics engineering, and the Ph.D. degree in power electronics all from the Technical University of Catalonia, Barcelona, Spain, in 1997, 2000, and 2003, respectively.
He was an Associate Professor with the Department of Automatic Control Systems and Computer Engineering, Technical University of Catalonia, where he currently teaches courses on digital signal processing, field-programmable gate arrays, microprocessors, and renewable energy. Since 2004, he has been responsible for the Renewable Energy Laboratory, Escola Industrial de Barcelona. He has been a visiting Professor at Zhejiang University, Hangzhou, China, and the University of Cergy-Pontoise, Pontoise, France. In 2012, he was the Guest Professor Chair at Nanjing University Aeronautics and Astronautics. Since 2011, he has been a Full Professor of microgrids at the Institute of Energy Technology, Aalborg University, Aalborg, Denmark, where he is the responsible of the microgrids research program. His research interests are oriented to different Microgrids aspects, including power electronics, distributed energy storage systems, hierarchical and cooperative control and energy management systems, and optimization of microgrids and islanded minigrids.